Characterization of Atmospheric Absorption in the 60 GHz Frequency Band Using a Multi-Pole Material Model

Müberra Arvas [1], Ercumend Arvas [1], and Mohammad A. Alsunaidi [2]

[1] Department of Electrical Engineering
Istanbul Medipol University, Istanbul, Turkey
marvas@st.medipol.edu.tr, earvas@medipol.edu.tr

[2] Electrical and Electronics Engineering Department
Marmara University, Istanbul, Turkey
mohammad.alsunaidi@marmara.edu.tr

Abstract ─ Atmospheric attenuation of electromagnetic signals at the 60 GHz frequency band is dominated by oxygen absorption which represents a major obstacle to 5G communications using this band. So far, only empirical equations that fit the experimental absorption data have been reported. These empirical models are not suitable to employ in standard full-wave electromagnetic simulators based on the numerical solution of Maxwell's equations. In this paper, a frequency-dependent material model for atmospheric absorption at the 60 GHz band is presented. Further, a numerical simulator that incorporates this multi-pole material dispersion model and uses the rotating boundary conditions to allow for long propagation distances is developed. The simulation algorithm is based on the auxiliary differential equation finite-difference time-domain (ADE-FDTD) technique which implements the general electric polarization formulation. The results are useful in the prediction of propagation power loss between line-of-sight communication links and in the planning and positioning of ground and air-borne facilities.

Index Terms ─ 5G communications, 60GHz frequency band, atmospheric attenuation, FDTD method, lorentz model, oxygen absorption.

I. INTRODUCTION

The demand for fast data transfer and large bandwidth is expected to grow further and further over the coming decades. This is in part due to the large number of multi-media applications that require real-time communications and processing, and in part due to the growing consumer expectations and demands. The fact that the unlicensed 60 GHz frequency band is a strong contender to satisfy such demands requires addressing important issues and challenges pertinent to this band. The sea level atmosphere is known for its significant attenuation of frequencies around 60 GHz due to high oxygen absorption. Oxygen absorption constitutes over 95% of this atmospheric attenuation which peaks around 60 GHz, with a value of over 15 dB/km. The successful adoption of 5G communications using the 60 GHz frequency band for wireless and radio communications relies on the introduction of novel antenna designs and communication strategies to overcome the channel loss. There has been a lot of emphasis on measurement [1,2] and modeling [3-6] techniques of atmospheric attenuation. The modeling effort focuses on the precise representation of the physical phenomena involving oxygen absorption lines at different atmospheric conditions. The final product of these models is customarily represented by a large verity of functions and polynomials (empirical fitting) with several physical parameters and mixing coefficients. The resulting empirical models are useful and can be utilized to approximate attenuation levels as a function of frequency and elevation. On the other hand, work has been done on the utilization of these models in solving real-life propagation problems. Grishin et al. used experimental data for atmospheric signal attenuation in an analytical model based on solving an inverse problem to simulate satellite signal propagation [7]. The work done in [8,9] simulated the signal absorption and dispersion due to the atmosphere by embedding the empirical relations into a transfer function and placed it in the channel part of the communication system. Other methods based on analytical solutions can in fact utilize these empirical functions but only for the treatment of simple propagation situations. Calculations based on the ray tracing method and the parabolic wave approximation have been proposed [10-13]. The ray tracing method is more suited for propagation problems with large-size features over a smooth ground in a homogeneous atmosphere. For complex environments, the computational time drastically increases and the accuracy deteriorates as the number of required rays

Submitted On: July 22, 2019
Accepted On: October 23, 2019

significantly increases. Also, the method fails for gazing angles. On the other hand, although the methods based on parabolic approximation are good for large distance propagation, they become less effective in solving problems involving complex terrain and strong atmospheric dispersion. Obviously, because empirical models representing the atmosphere involve complicated expressions and functions, analytical methods become limited in application. Instead, the empirical models need to be incorporated into standard full-wave electromagnetic simulators using, for example, the finite-difference time-domain method (FDTD) and the finite-element method (FEM).

The objective of this work is three-fold. First, a material model of atmospheric attenuation is developed by fitting measurement data to standard Lorentz poles. The reason behind this choice is that Lorentz functions represent the most general matter-wave interaction forms. Second, the material model is incorporated in the time-domain simulations of Maxwell's equations and specifically in a FDTD algorithm. This objective is achieved through the general polarization formulation and the auxiliary differential equation (ADE) technique [14,17]. Finally, simulations of long-distance propagations in the 60 GHz frequency band are carried out. To the best of our knowledge, this is the first report of incorporating atmospheric attenuation in a FDTD algorithm using the Lorentz model. This model should find applications in many disciplines, including remote sensing, geophysical mapping and in point-to-point communications, where it can help in planning the positions of ground and air-borne facilities.

II. ATMOSPHERIC MATERIAL MODEL

The frequency-dependent behavior of dispersive materials can be described by the constituent relations. For non-magnetic materials, the electric polarization is used to represent the dielectric effects inside the material. Assuming a linear material response, the frequency-dependent electric flux density can be written as:

$$\vec{D}(\omega) = \varepsilon_o \varepsilon_\infty \vec{E}(\omega) + \vec{P}(\omega), \quad (1)$$

where $\boldsymbol{\varepsilon_o}$ is the free space permittivity, $\boldsymbol{\varepsilon_\infty}$ is the high frequency dielectric constant and $\boldsymbol{\omega}$ is the frequency. The first order linear polarization $\boldsymbol{P(\omega)}$ is related to the electric field intensity, $\boldsymbol{E(\omega)}$, in the frequency domain by the electric susceptibility as:

$$P(\omega) = \varepsilon_o \, \chi(\omega) \, E(\omega). \quad (2)$$

Combining equation (1) and equation (2), one can write:

$$\varepsilon_r(\omega) = \varepsilon_\infty + \chi(\omega), \quad (3)$$

where $\boldsymbol{\varepsilon_r(\omega)}$ is the frequency-dependent complex relative permittivity of the dispersive material. The dispersion relation for the electric susceptibility $\boldsymbol{\chi(\omega)}$ that represents the material-wave interaction can be represented by a general Lorentz model function of the form:

$$\chi(\omega) = \frac{\mathbf{a}}{\mathbf{b} + jc\omega - \mathbf{d}\omega^2}, \quad (4)$$

where **a**, **b**, **c** and **d** are model parameters that can be obtained from material properties or by fitting to experimental data. The atmospheric material model developed in this work is based on a recent report by the International Telecommunication Union [2]. The report provides empirical methods to estimate the attenuation of atmospheric gases on terrestrial and slant paths using experimental data. In the report, an estimate of gaseous attenuation computed by summation of individual absorption lines for the frequency range 1 GHz to 1 THz is given. Figure 1 is a reproduction of the atmospheric specific attenuation using several empirical formulae given in [2] for frequencies between 40 and 80 GHz. The curve in Fig. 1 is based on atmospheric conditions of dry air with total air pressure of 1033.6 hPa and average temperature of 15 °C.

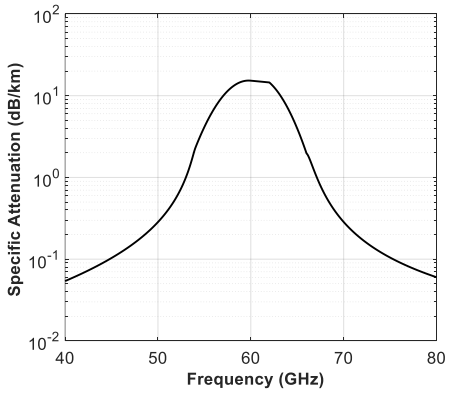

Fig. 1. Atmospheric specific attenuation for the 40-80 GHz frequency range at sea level, as given by the empirical formulae in [2].

In this work, a fitting to the general Lorentz poles is performed. The strategy for using the experimental data is as follows. For any given frequency range and elevation, frequency-dependent complex permittivity values are obtained from attenuation readings using the following relations:

$$\varepsilon_r' = (n')^2 + (n'')^2, \quad (5\text{-}1)$$

$$\varepsilon_r'' = -\alpha n' v/\omega, \quad (5\text{-}2)$$

where $\boldsymbol{n'}$ and $\boldsymbol{n''}$ are the real and imaginary parts of the complex refractive index, respectively, $\boldsymbol{\alpha}$ is the attenuation coefficient and $\boldsymbol{v}$ is the speed of light. Those complex permittivity data are fitted to standard material models with as many poles as necessary. Out of the fitting process, the required parameters for the time-domain simulator are obtained. Here, a Lorentzian dielectric function of the form:

$$\varepsilon_r(\omega) = \varepsilon_\infty + (\varepsilon_s - \varepsilon_\infty)\sum_{i=1}^{M} \frac{A_i\omega_i^2}{\omega_i^2 + j2\delta_i\omega - \omega^2}, \quad (6)$$

is used, with $\mathbf{a_i} = (\boldsymbol{\varepsilon_s} - \boldsymbol{\varepsilon_\infty})\boldsymbol{A_i\omega_i^2}$, $\mathbf{b_i} = \boldsymbol{\omega_i^2}$, $\mathbf{c_i} = \mathbf{2}\boldsymbol{\delta_i}$ and $\mathbf{d_i} = \mathbf{1}$ being the parameters in equation (4). In equation (6), $\boldsymbol{\varepsilon_s}$ is the effective static dielectric constant, $\boldsymbol{A_i}$ is the pole strength, $\boldsymbol{\omega_i}$ is the resonance frequency and $\boldsymbol{\delta_i}$ is the damping parameter for i^{th} pole. M represents the total number of poles of the material dispersion relation.

The fitting process to Lorentzian poles goes as follows. One can start with a Lorentzian pole that has a peak around the center of the curve in Fig. 1 (i.e., around 60 GHz). This step yields the value of the resonance frequency of the first pole. Next, to accommodate for the width of the spectrum of the measurement data, other poles at above and below the first resonance frequency are added. Finally, the values of the pole strength and damping parameter for each pole are adjusted such that a reasonable fit is obtained. Table 1 shows the *a*, *b*, *c* and *d* parameters for the three Lorentz poles used for atmospheric attenuation modeling. These parameters are related to the pole parameters using equation (6). The resulting dielectric function (real and imaginary parts) is shown in Fig. 2, together with the reference measurement data. The fitting is good in general, and focus has been made on the frequency range around 60 GHz where the expected bandwidth of the transmitting antenna is located. The obtained poles form the basis for the relation between the electric polarization and the electric field.

Next, the frequency-domain dielectric function is incorporated in a time-domain simulator using the ADE-FDTD method. Equation (2) can be expressed in the time domain using the Fourier transform, as reported in [16]. The procedure results in a second order differential equation for the electric polarization vector given by:

$$\mathbf{b}P + \mathbf{c}\frac{d}{dt}P + \mathbf{d}\frac{d^2}{dt^2}P = \mathbf{a}\,\varepsilon_o E. \quad (7)$$

Using finite-difference approximations, the time domain update equation for the linear polarization in equation (7) becomes:

$$P^{n+1} = C_1P^n + C_2P^{n-1} + C_3E^n. \quad (8)$$

The constants in equation (8) are given by:

$$C_1 = \frac{4\mathbf{d}}{2\mathbf{d}+\mathbf{c}\Delta t+\mathbf{b}\Delta t^2}, \quad (9\text{-}1)$$

$$C_2 = \frac{-2\mathbf{d}+\mathbf{c}\Delta t-\mathbf{b}\Delta t^2}{2\mathbf{d}+\mathbf{c}\Delta t+\mathbf{b}\Delta t^2}, \quad (9\text{-}2)$$

$$C_3 = \frac{2\mathbf{a}\varepsilon_o\Delta t^2}{2\mathbf{d}+\mathbf{c}\Delta t+\mathbf{b}\Delta t^2}, \quad (9\text{-}3)$$

where n is the time index and $\boldsymbol{\Delta t}$ is the time step. It should be noted that in deriving the expressions in equation (9), semi-implicit finite-differencing has been used. In this case, the first term on the right-hand side of equation (7) was approximated using the average of $\boldsymbol{P^{n-1}}$ and $\boldsymbol{P^{n+1}}$ time instances. This scheme is known to improve the stability of the overall algorithm, even with strong dispersion. All field components and parameters are arranged on the FDTD computational grid using the standard Yee's cell. The time-domain algorithm proceeds as follows. First, the electric flux densities are evaluated using Maxwell's curl equation with available magnetic field samples. Next, the linear polarization vector is updated using equation (8). Third, the electric field intensity components are updated using the time-domain version of equation (1) as:

$$E^{n+1} = \frac{D^{n+1} - \sum_{i=1}^{M} P_i^{n+1}}{\varepsilon_o\varepsilon_\infty}. \quad (10)$$

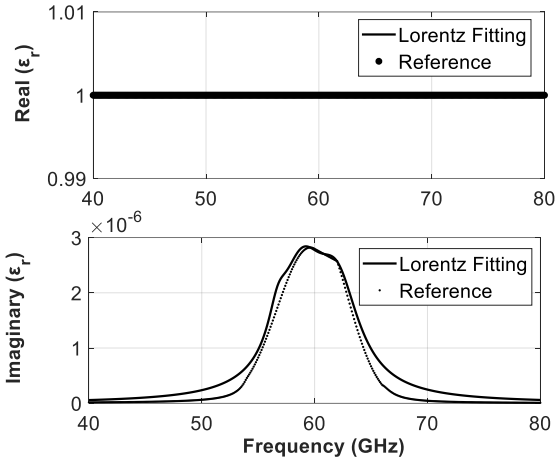

Fig. 2. Real and imaginary dielectric constant curves as obtained from the empirical attenuation function (Ref 2, dashed line) and the corresponding 3-pole Lorentz fit (solid line) for sea level atmospheric conditions.

Table 1: Lorentz pole parameters for atmospheric attenuation at sea level

Pole $\boldsymbol{i}$	$\mathbf{a}_i$ **(rad/s)²**	$\mathbf{b}_i$ **(rad/s)²**	$\mathbf{c}_i$ **(rad/s)**	$\mathbf{d}_i$
1	2.0245×10^{16}	1.5210×10^{23}	3.0×10^{10}	1
2	2.4546×10^{16}	1.3690×10^{23}	3.2×10^{10}	1
3	2.7960×10^{15}	1.2709×10^{23}	1.2×10^{10}	1

Finally, the second Maxwell's curl equation is used to calculate the magnetic field components. The flowchart in Fig. 3 describes the sequence of calculations in the resulting algorithm. It is important to mention here that solving this problem using the classical ADE algorithm [18] would introduce higher order time derivatives, the solution of which would require matrix inversion. When applied to the problem presented in this work with three Lorentzian poles, derivatives of the sixth order result. It would be necessary to save a large number of time samples and hence, using a mixed explicit-implicit scheme, matrix inversion is needed. The FDTD algorithm used here is significantly more efficient and robust. Other ADE algorithms reported in literature

require complex-domain operations (for example [19]). In general, complex-domain operations require twice as much computation time and memory storage as normal real operations. The computational requirements are clearly a function of the number of poles of the dispersion model. For multi-pole dispersion problems, these FDTD algorithms would require more constants to be evaluated and stored in memory.

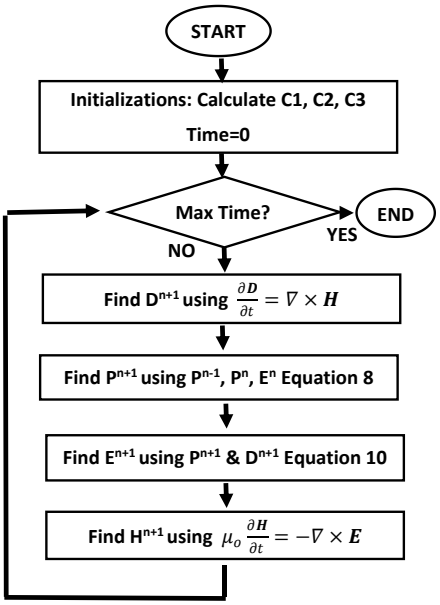

Fig. 3. Flowchart of the calculation sequence in the time-domain algorithm.

III. SIMULATION RESULTS

To test wave propagation using the proposed atmosphere model, the FDTD simulation algorithm presented in section II is implemented. A time-limited pulse of a Gaussian form given by:

$$A(t) = A_o \exp\left[-\left(\frac{t-t_o}{t_p}\right)^2\right] \cos[\omega_c(t-t_o)], \quad (11)$$

is used as a point-source excitation, where A_o is the initial pulse amplitude, t is time variable, t_o is the offset time, t_p is the pulse waist and ω_c is the central frequency. The parameter t_p is used to steer the frequency contents of the pulse. In this work, a pulse waist of 20 picoseconds is used such that it covers a large frequency band around 60 GHz, which is taken as the central frequency ω_c. A plane wave propagation in a one-dimensional sea-level atmosphere is considered. The value of the spatial step is set to a very small fraction of the smallest wavelength involved in propagation. This is required to ensure that numerical dispersion is significantly minimized, and that channel dispersion is correctly represented. Accordingly, a spatial step size of 0.01 mm is used. The stability of the algorithm is determined by the standard Courant-Friedrichs-Lewy (CFL) condition for the FDTD method, which is given by [15]:

$$\Delta t \leq \frac{1}{v_{\max}\sqrt{\frac{1}{\Delta x^2}+\frac{1}{\Delta y^2}+\frac{1}{\Delta z^2}}}. \quad (12)$$

A time step of 0.03 picoseconds satisfies this condition. Numerical dispersion is an artifact of the approximation of the spatial derivatives in finite differences. Because the spatial step is finite, errors in data transmission throughout the computational grid propagate and accumulate. The general guideline is to make the spatial step a very small fraction of the smallest wavelength involved in the propagation. This problem becomes more serious if the medium of propagation is itself dispersive. Consequently, with high levels of space resolution, the memory requirement for the simulation of hundreds of meters of propagation distance becomes unaffordable. To solve this problem, the rotating boundary conditions have been used. In this case, as shown in Fig. 4, the pulse propagates across the whole domain, exits the computational window from one boundary and re-enters from the other boundary to start propagating the domain again.

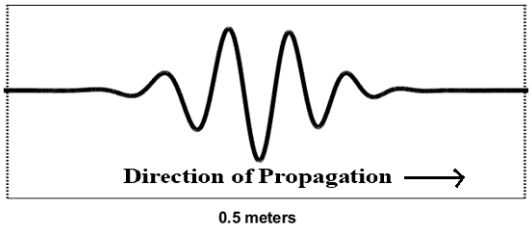

Fig. 4. Pulse propagation in rotating boundary conditions. The total length of the computational window is half a meter.

The rotating boundary conditions are thus defined as follows. For the first Maxwell's equation, the curl is evaluated in one-dimensional case using:

$$\left.\frac{\partial D}{\partial t}\right|_{i=i_1} = \frac{H(i_1)-H(i_{\max-1})}{\Delta x}, \quad (13)$$

and

$$\left.\frac{\partial D}{\partial t}\right|_{i=i_{\max}} = \frac{H(i_{\max-1})-H(i_1)}{\Delta x}. \quad (14)$$

In equations (12) and (13), i_1 and i_{max} are the first and last points in the computational domain, and Δx is the spatial step. The curl in the second Maxwell's equation is treated similarly. The initial size of the computational domain is set to half a meter. The choice of this initial domain size ensures that it is wide enough to comfortably accommodate the pulse at any time throughout the simulation, even with the resulting dispersion due to the channel. The pulse transpasses the computational domain for multiples of times to achieve a certain propagation distance. In this study, the pulse is propagated well over one kilometer. Also, a reference simulation in a lossless atmosphere was carried out such

that comparisons are possible. Figure 5 shows the time-domain electric field waveform for the propagating pulse at 1000 meters. The reference waveform for a lossless atmosphere is also shown in the figure. The attenuation and dispersion of the pulse is evident. Power calculations have been performed to validate the numerical model. The spectrum of the received signal power has been produced after propagation of 1000 m. At any given location, the power density is given by:

$$\vec{S} = \frac{1}{2}\vec{E} \times \vec{H}^*. \quad (15)$$

For a wave propagating along the x direction, the spectrum of the real power density is given by:

$$S(f)_{x,r} = \frac{1}{2}\left[E(f)_{y,r}H(f)_{z,r} + E(f)_{y,i}H(f)_{z,i}\right], \quad (16)$$

where the subscripts r and i denote the real and imaginary parts, respectively. The amount of received power at several distances are shown in Fig. 6. It is clearly seen from the figure that a signal at 60 GHz loses more than 97% of its initial power within the first kilometer. The propagation of the 50, 60 and 70 GHz frequency components are shown separately in Fig. 7, where normalization has been made to the input value for each frequency component. Table 2 and Fig. 8 show the comparison between the amount of loss per kilometer, as given by the reference attenuation curve (Fig. 1) and by the FDTD simulation, for selected frequencies. The slight discrepancies in the power loss are attributed to the imperfections in the fitting process.

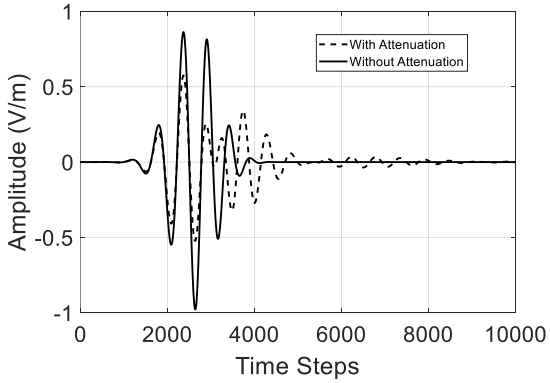

Fig. 5. Time profile of the received electric field at a distance of 1000 meters, with and without attenuation.

Table 2: Loss comparison between simulation results and reference data

Frequency (GHz)	Loss (dB/km)	
	Reference	Simulation
57	8.78	9.00
58	11.43	11.42
59	15.23	14.26
60	15.26	16.04
61	14.89	14.61
62	14.51	11.93
63	10.75	9.61

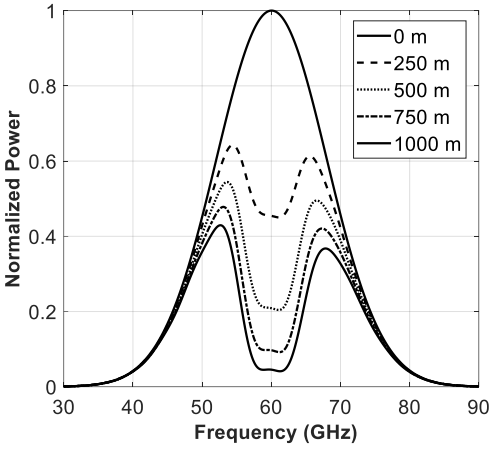

Fig. 6. Normalized signal power at different propagation distances versus frequency.

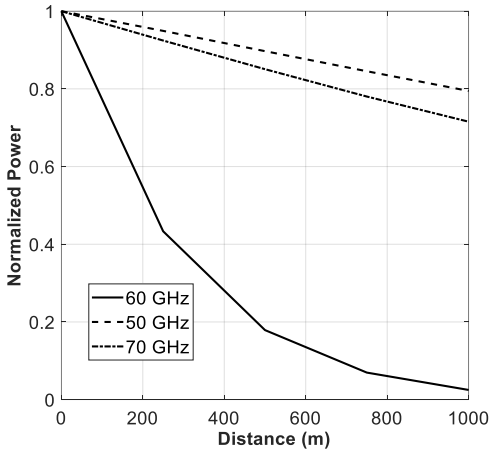

Fig. 7. Normalized received power for the 50, 60 and 70 GHz frequency components versus distance.

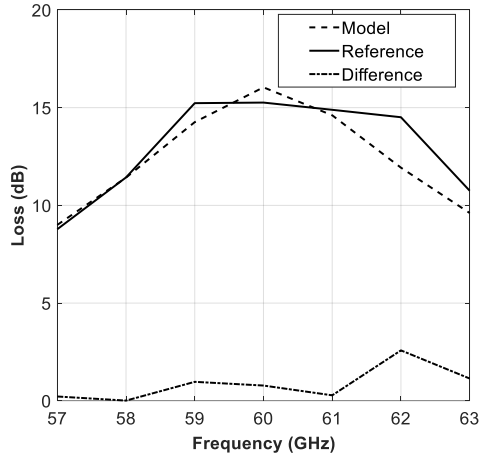

Fig. 8. Estimated loss after propagation of 1000 meters, as given by the simulation model. The reference values and the difference are shown for comparison.

IV. CONCLUSION

A propagation model for atmospheric absorption of 60 GHz band signals has been presented. The model is incorporated in an FDTD numerical simulator as a multi-pole material dispersion term using the ADE technique. The rotating boundary conditions have been used to allow for long propagation distances. Also, the validity of the model has been demonstrated. This model is very useful in the study of many situations involving free space communications with the possibility of incorporating different scenarios, such as reflections from buildings, presence of ground, terrain and water bodies and interference. It can be added to commercial electromagnetic software packages as a separate material module. The results are also useful in the prediction of propagation power loss such that methods for loss compensation can be devised. Work is underway to model atmospheric attenuation at different elevations and different weather conditions.

REFERENCES

[1] D. S. Makarov, M. Y. Tretyakov, and P. W. Rosenkranz, "60-GHz oxygen band: Precise experimental profiles and extended absorption modeling in a wide temperature range," *Journal of Quantitative Spectroscopy & Radiative Transfer*, 112, pp. 1420-1428, 2011.

[2] International Telecommunication Union, *Attenuation by atmospheric gases*, Recommendation ITU-R P.676-9, 02/2012.

[3] H. J. Liebe, "MPM: An atmospheric millimeter-wave propagation model," *International Journal of Infrared and Millimeter Waves*, 10.6, pp. 631-650, 1989.

[4] M. Y. Tretyakov, M. Koshelev, V. Dorovskikh, D. S. Makarov, and P. W. Rosenkranz, "60-GHz oxygen band: Precise broadening and central frequencies of fine-structure lines, absolute absorption profile at atmospheric pressure, and revision of mixing coefficients," *Journal of Molecular Spectroscopy*, 231, 1-14, 2005.

[5] G. Frank, J. Wentz, and T. Meissner, "Atmospheric absorption model for dry air and water vapor at microwave frequencies below 100 GHz derived from spaceborne radiometer observations," *Radio Sci.*, 51, 2016.

[6] B. T. Nguyen, A. Samimi, and J. J. Simpson, "Recent advances in FDTD modeling of electromagnetic wave propagation in the ionosphere," *ACES Journal*, vol. 29, no. 12, pp. 1003-1012, Dec. 2014.

[7] D. V. Grishin, D. Y. Danilov, and L. Kurakhtenkov, "Use of ITU-R recommendations in calculating tropospheric signal attenuation in the simulation modeling problems of satellite systems," *Systems of Signal Synchn. Generating and Processing in Telecomm*, pp. 1-4, 2017.

[8] A. C. Valdez, "Analysis of Atmospheric Effects due to Atmospheric Oxygen on a Wideband Digital Signal in the 60 GHz Band," *Master's thesis*, *Virginia Polytechnic Institute*, 2001.

[9] A. Chinmayi, M. Vasanthi, and T. Rama Rao, "Performance evaluation of RF based Inter satellite communication link at 60 GHz," *International Conference on Wireless Communications, Signal Processing and Networking*, India, Mar. 2016.

[10] J. G. Powers, J. B. Klemp, W. C. Skamarock, C. A. Davis, J. Dudhia, D. O. Gill, J. L. Coen, and D. J. Gochis, "The weather research and forecasting model: Overview, system efforts, and future directions," *American Meteorological Society*, vol. 98, no. 8, pp. 1717-1737, 2017.

[11] A. E. Barrios, "A terrain parabolic equation model for propagation in the troposphere," *IEEE Transactions on Antennas and Propagation*, vol. 42, no. 1, pp. 90-98, 1994.

[12] J. Kuttler and G. D. Dockery, "Theoretical description of the parabolic approximation/Fourier split-step method of representing electromagnetic propagation in the troposphere," *Radio Science*, vol. 26, no. 02, pp. 381-393, 1991.

[13] H. Zhou, A. Chabory, and R. Douvenot, "A 3-D split-step Fourier algorithm based on a discrete spectral representation of the propagation equation," *IEEE Transactions on Antennas and Propagation*, vol. 65, no. 4, pp. 1988, 1995, 2017.

[14] M. A. Eleiwa and A. Z. Elsherbeni, "Debye constants for biological tissues from 30 Hz to 20 GHz," *ACES Journal*, vol. 16, no. 3, Nov. 2001.

[15] Atef Elsherbeni and Veysel Demir, *The Finite Difference Time Domain Method for Electromagnetics with MATLAB Simulations*, Second Edition, Edison, NJ, 2015.

[16] M. A. Alsunaidi and A. Al-Jabr, "A general ADE-FDTD algorithm for the simulation of dispersive structures," *IEEE Photonics Tech. Lett.*, vol. 21, no. 12, pp. 817-819, June 2000.

[17] M. Arvas and M. A. Alsunaidi, "A multi-pole model for oxygen absorption of 60 GHz frequency band communication signals," *The Computational Methods and Telecommunication in Electrical Engineering and Finance, Sarajevo*, pp. 92-94, May 6-9, 2018.

[18] A. Taflove, *Computational Electrodynamics: The Finite-Difference Time-Domain Method*, Artech House, Norwood, MA, 1995.

[19] M. Han, R. Dutton, and S. Fan, "Model dispersive media in finite-difference time-domain method with complex-conjugate pole-residue pairs," *IEEE Microw. Wireless Compon. Lett.*, 16, pp. 119-121, 2006.

Ercumend Arvas received the B.S. and M.S. degrees from the Middle East Technical University, Ankara, Turkey in 1976 and 1979, respectively, and the Ph.D. degree from Syracuse University, Syracuse, NY in 1983, all in Electrical Engineering. From 1984 to 1987, he was with the Electrical Engineering Department, Rochester Institute of Technology, Rochester, NY. He was with the EE Department of Syracuse University between 1987 and 2014. He is currently a Professor in the EE Department of Istanbul Medipol University. His research and teaching interests are in electromagnetic scattering and microwave devices. Arvas is a Member of the Applied Computational Electromagnetics Society (ACES), and Fellow of IEEE and Electromagnetics Academy.

M. A. Alsunaidi is currently a Visiting Professor at the Electrical and Electronics Engineering Department of Marmara University, Istanbul, Turkey. His main areas of reaserch are optoelectronics and computational electromagnetics. His fields of interest include antenna design, solid-state lighting and plasmonics.

Muberra Arvas has joined Prof. Ercumend Arvas' project group in 2015. She is currently doing her M.S.E.E under the supervision of Prof. Ercumend Arvas, in Istanbul Medipol University, Turkey. Her current research areas are antennas and numerical electromagnetics.